Elastic, Electronic, Optical and Thermal Properties of Na2Po: An Ab Initio Study

Article *in* Journal of Electronic Materials · October 2015

DOI: 10.1007/s11664-015-4119-4

CITATIONS
0

READS
548

8 authors, including:

Eithiraj R. D
VIT University
21 PUBLICATIONS **160** CITATIONS
SEE PROFILE

H. Khachai
University of Sidi-Bel-Abbes
46 PUBLICATIONS **248** CITATIONS
SEE PROFILE

Rabah Khenata
University Mustapha Stambouli of Mascara
514 PUBLICATIONS **4,006** CITATIONS
SEE PROFILE

Ghulam Murtaza
Islamia College Peshawar
131 PUBLICATIONS **768** CITATIONS
SEE PROFILE

Journal of ELECTRONIC MATERIALS, Vol. 45, No. 1, 2016
DOI: 10.1007/s11664-015-4119-4

Elastic, Electronic, Optical and Thermal Properties of Na_2Po: An *Ab Initio* Study

N. BAKI,[1] R.D. EITHIRAJ,[2,7] H. KHACHAI,[1] R. KHENATA,[3,8] G. MURTAZA,[4] A. BOUHEMADOU,[5] T. SEDDIK,[3] and S. BIN-OMRAN[6]

1.—Laboratoire d'étude des Matériaux et Instrumentations Optiques-Faculté des Sciences Exactes, Djillali Liabès University, 22000 Sidi Bel Abbès, Algeria. 2.—Crystal Growth & Crystallography Division, School of Advanced Sciences, VIT University, Vellore 632 014, Tamil Nadu, India. 3.—Laboratoire de Physique Quantique et de Modélisation Mathématique, Université de Mascara, 29000 Mascara, Algeria. 4.—Materials Modeling Lab, Department of Physics, Islamia College University, Peshawar, Pakistan. 5.—Laboratory for Developing New Materials and their Characterization, Department of Physics, Faculty of Science, University of Setif, 19000 Setif, Algeria. 6.—Department of Physics and Astronomy, College of Science, King Saud University, P.O.Box 2455, Riyadh 11451, Saudi Arabia. 7.—e-mail: eithiraj.rd@vit.ac.in. 8.—e-mail: khenata_rabah@yahoo.fr

The structural, elastic, electronic, optical and thermodynamic properties of the sodium polonide Na_2Po compound have been studied through the full potential linearized augmented plane wave plus local orbitals (FP-LAPW + lo) and tight-binding linear muffin-tin orbital (TB-LMTO) methods. The exchange–correlation potential was treated within the local density approximation for the TB-LMTO calculations and within the generalized gradient approximation for the FP-LAPW + lo calculations. In addition, Tran and Blaha-modified Becke–Johnson (TB-mBJ) potential and Engel–Vosko generalized gradient approximation were used for the electronic and optical properties. Ground state properties such as the equilibrium lattice constant, bulk modulus and its pressure derivative were calculated and compared with available data. The single-crystal and polycrystalline elastic constants of the considered compound were calculated via the total energy versus strain in the framework of the FP-LAPW + lo approach. The calculated electronic structure reveals that Na_2Po is a direct band gap semiconductor. The frequency-dependent dielectric function, refractive index, extinction coefficient, reflectivity coefficient and electron energy loss function spectra are calculated for a wide energy range. The variations of the lattice constant, bulk modulus, heat capacity, volume expansion coefficient and Debye temperature with temperature and pressure were calculated successfully using the FP-LAPW + lo method in combination with the quasi-harmonic Debye model.

Key words: Electronic structure, band gap, optoelectronic, FP-LAPW + lo, TB-LMTO

INTRODUCTION

The sodium chalcogenides Na_2A (A: S, Se and Te) compounds are narrow direct band gap semiconductors[1,2] crystallizing in the cubic anti-fluorite structure (anti-CaF_2-type), space group No. 225.[3] They appear promising for technological application in solid-state batteries, fuel cells, solid-state gas detectors and photo-emissive ultraviolet (UV) light materials.[4–7] Therefore, these materials have been the subject of numerous experimental and theoretical studies. Experimentally, the elastic constants of the Na_2S compound have been determined using an elastic neutron scattering technique at low temperature by Bührer and Bill.[8] Bertheville et al.[9]

(Received May 4, 2015; accepted September 30, 2015; published online October 19, 2015)

measured the ionic conductivity of Na_2S, and showed that this compound exhibits a super-ionic behavior at a temperature close to the melting point, confirming the suggestion of Bührer and Bill.[10] Theoretically, the ground state and high-pressure phases of Na_2S were studied up to a pressure of 100 GPa using Hartree–Fock and density-functional theory.[11] The structural, electronic and elastic properties of sodium chalcogenides Na_2A (A: S, Se and Te) were reported by many authors.[1,10,12–15] The lattice dynamics properties of the Na_2A (A: S, Se and Te) compounds were reported by Kalarasse et al.[16] The structural, electronic and optical properties of alkali metal telluride Na_2Te were investigated in the framework of density functional theory (DFT) within generalized gradient approximation (GGA) by Alay-e-Abbes and Shaukat.[17] Recently, a first-principle study on the lattice dynamics, thermodynamics and elastic properties of Na_2Te under high pressure were performed by Zhang and co-workers[7] using a pseudopotential plane-wave approach based on DFT. These compounds constitute a good example for a homologous series of crystals with predictable physical and physicochemical properties.

Although there has been considerable progress in the theoretical description of the structural and electronic properties of the sodium chalcogenides Na_2A (A: S, Se, Te) compounds, there is a real lack of knowledge about the electronic, elastic, optoelectronic and thermal properties of the fourth member of the series, namely the sodium polonide Na_2Po; they are still not investigated experimentally or theoretically, which has prompted us to study them through accurate *ab initio* calculations. Therefore, the present work aims to study the structural, elastic, electronic, optical and thermodynamic properties of Na_2Po in order to provide the data currently lacking for Na_2Po.

COMPUTATIONAL DETAILS

The first part of the present calculations was performed using the full potential linearized augmented plane wave plus local orbitals (FP-LAPW + lo) method[18,19] in the framework of the DFT,[20,21] as implemented in the Wien2K code,[22] which is one of the most accurate and effective methods for the calculation of the ground state properties of materials.[23,24] In this method, the crystal unit cell is partitioned into non-overlapping muffin-tin (MT) spheres which surround each of the atomic and interstitial regions. Inside the MT sphere, which is centered at each atomic nucleus, the electronic wave functions and crystal potential were expanded in a basis set of spherical harmonics, while for the interstitial region, the electronic wave functions were expanded in a basis set of plane waves. The exchange–correlation contribution is treated within the generalized gradient approximation as proposed by Perdew, Burke and Ernzerhof (GGA-PBE)[25] for the calculations of the structural, elastic and thermodynamic properties. On the other hand, for the calculation of the electronic and optical properties, in addition to the GGA-PBE approximation, the Engel–Vosko generalized gradient approximation (EV-GGA)[26] and the recent Tran and Blaha-modified Becke–Johnson potential (TB-mBJ)[27] were also applied. The muffin-tin radii (R_{MT}) of 2.0 and 2.25 atomic units (*a.u.*) were used for the Na and Po atoms, respectively. In order to ensure convergence of the computed total energy, the wave functions in the interstitial region were expanded in plane waves with a cut-off R_{MT} $K_{max} = 9$, where R_{MT} denotes the smallest MT radius and K_{max} designate the magnitude of the largest K vector in the plane wave expansion. Inside each MT sphere, the electronic functions were expanded in a basis set of spherical harmonics up to the angular momentum of $l_{max} = 10$. The integrals over the Brillouin zone (BZ) were performed using the $12 \times 12 \times 12$ k-point grid for the calculation of the structural and electronic properties, while for the optical properties, a mesh of $20 \times 20 \times 20$ k-points was used following the Monkhorst–Pack special k-point sampling.[28] The self-consistent iteration process was repeated until the total energy convergence was less than 10^{-5} Ry.

The second part of the present calculations was carried by using Andersen's tight-binding version of the TB-LMTO method[29,30] within the local density approximation (LDA) of von Barth and Hedin parameterization[31] to investigate the total energy and electronic structure. The atomic sphere approximation (ASA) has been used where the Wigner–Seitz sphere radii are chosen in such a way that the potential discontinuity at the sphere boundary is a minimum and the charge flow between the atoms is in accordance with the electronegativity criteria. Additionally, the overlaps of the atomic spheres are kept within 16%. The total energy convergence was well-checked by increasing the number of k-points where the band structure calculations were performed for 512 k-points. In addition, the tetrahedron method of Brillouin zone integration has been used to calculate the density of states (DOS).[32]

The knowledge of specific behaviours of materials when they are under severe constraints, such as in high-pressure and high-temperature environments, is of great importance for technological applications. To address this interest in the present work, the pressure and temperature dependencies of the lattice parameter, bulk modulus, volume expansion coefficient, heat capacity and the Debye temperature of the Na_2Po compound were investigated using the FP-LAPW + lo method combined with the quasi-harmonic Debye model as implemented in the Gibbs code.[33]Further details of this procedure can be found in other published articles.[34,35]

RESULTS AND DISCUSSION

Structural Properties

In order to calculate the structural ground-state properties of sodium polonide, the total energies (E) were calculated as a function of the primitive-cell volume (V), which ranges from 1.25 V_{expt} to 0.55 V_{expt}, where V_{expt} is the experimental value of the primitive cell.[36] The total energies versus primitive-cell volume of the sodium polonium compound are given in Fig. 1, where the calculated E–V data were fitted to the Birch equation of state[37] to obtain the structural equilibrium properties, such as the equilibrium lattice constant a, bulk modulus B_0 and its pressure derivative B'. Table I shows the theoretically calculated equilibrium lattice constant a, bulk modulus B_0 and pressure derivative of the bulk modulus B' together with the available data in the literature, where the calculated value of the equilibrium lattice constant (a) is in good agreement with the measured one.[36] As it has already been emphasized in the Introduction section, the sodium polonium crystal is relatively less explored; hence (to the best of our knowledge), there are currently no reported values in the literature for comparison with the calculated bulk modulus B_0 and its pressure derivative B'. In addition, the results from the present study and that of Ref. 16 show that the lattice constant (a) increases for the series of the Na_2Ch compounds (where Ch = S, Se, Te, Po), and when the Ch element varies by going downwards in the periodic table column from the element S to Po. This is an expected result since the values of the atomic radii (R) of the Ch atoms are given by :R(S) = 1.09 Å < R(Se) = 1.22 Å ≪ R(Te) = 1.42 Å < R(Po) = 1.68 Å. Similarly, the value of the isothermal bulk modulus B_0 decreases in the series of the Na_2Ch compounds, which is due to the fact that B_0 is inversely proportional to V_0, expressed as $B_0 \propto V_0^{-1}$, where V_0 is the volume of the unit cell. Furthermore, the relatively lower value of the B_0parameter corresponding to the Na_2Po compound shows that this compound can be classified as a soft material with high compressibility.

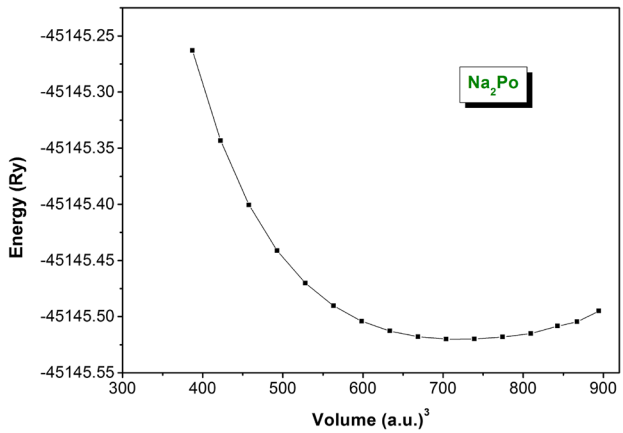

Fig. 1. Variation of the total energy versus the unit cell volume for the Na_2Po crystal using the GGA-PBE.

Elastic Constant

The second-order elastic constant, C_{ij} for the cubic Na_2Po compound at zero pressure and zero temperature was calculated using the variation of the unit cell total energy versus strain approach as proposed by Mehl,[38] where only small lattice distortions were applied in order to remain within the elastic domain of the crystal. A cubic structure is characterized by three independent elastic constants, namely, the C_{11}, C_{12}, and C_{44} constants, where the calculated values of the elastic constants, C_{ij} corresponding to the Na_2Po compound are listed in Table II. To the best of the authors' knowledge, elastic constants for the Na_2Po compound have not yet been previously obtained through experimental or theoretical methods; hence, our results can serve as a reference for future investigations.

From Table II, it is observed that the calculated elastic constants satisfy the conditions required for the mechanical stability of a cubic structure[39]:

$$C_{11} - C_{12} > 0,\ C_{44} > 0 \text{ and } C_{11} + 2C_{12} > 0. \quad (1)$$

Hence, the Na_2Po compound is mechanically stable. Furthermore, the calculated values of the elastic constants, C_{11}, C_{12} and C_{44} of the Na_2Po compound are lower than those of the Na_2S, Na_2Se and Na_2Te compounds,[16] thus indicating the decrease of the strengths of the series Na_2A compounds (where A = S, Se, Te, Po) in the following sequence $Na_2S \rightarrow Na_2Se \rightarrow Na_2pe \rightarrow Na_2Po$.

From the C_{ij} constants of a compound, some of its important properties such as the stiffness, brittle/ductility nature and type of chemical bonding can be estimated. Numerous macroscopic elastic

Table I. Calculated lattice constant (a, in Å), bulk modulus (B_0, in GPa) and its pressure derivative (B') for the Na_2Po crystal in the anti-fluorite-type structure

	a	B_0	B'
Present work	7.528[a]	17.87[a]	3.53[a]
	7.442[b]	17.20[b]	
Expt.[36]	7.473		

[a]Using the FP-LAPW method.[b]Using the TB-LMTO method.

Table II. Calculated elastic constants (C_{11}, C_{12} and C_{44}, in GPa), Young's modulus (E, in GPa), shear modulus (G, in GPa), Poisson's ratios (v, dimensionless), anisotropy factor (A) and B/G ratio for the Na_2Po compound using the FP-LAPW method within the GGA-PBE

C_{11}	C_{12}	C_{44}	B	G	E	v	A	B/G
29.61	12.0	8.78	17.87	8.79	22.66	0.28	0.999	2.03

The value of B is derived from the elastic constants using the well-known relation: the value of $\boldsymbol{B} = (\boldsymbol{C_{11} + 2C_{12}})/\boldsymbol{3}$.

moduli parameters such as the shear modulus G, Young's modulus E, Poisson's ratio v, anisotropy factor A and the Pugh's B/G ratio were calculated and presented in Table II. The Young's modulus E, which is defined as the ratio of stress over strain, is representative of the stiffness of a material where a greater E value indicates that the material is stiffer. Hence, the calculated value of E (from Table II) indicates that the Na_2Po compound has lower stiffness. Conversely, the value of the Poisson's ratio, v for a covalent material is small (where v = 0.1), whereas for an ionic material, the typical value of v is 0.25.[40] For the Na_2Po compound, the corresponding value of v is about 0.28, thus indicating a strong ionic contribution in the intra-atomic bonding for this compound. According to Pugh's empirical criterion,[41] a high and low B/G ratio may be associated with a ductile and brittle nature for a particular compound, respectively, and the critical value separating ductile and brittle materials is around 1.75.[41] For the Na_2Po compound, the calculated value of the B/G ratio is about 2.03, thus indicating that the investigated compound can be classified as a ductile material.

Although the investigated Na_2Po compound crystallizes in a cubic system, this does not necessarily imply that it should exhibit isotropic elastic properties where the elastic anisotropy has great importance for many mechanical-physical properties[42] in a compound. Moreover, recent research[43] demonstrates that elastic anisotropy has a significant influence on the nanoscale precursor textures in alloys. Therefore, several indexes have been developed to estimate the elastic anisotropy of materials where the anisotropic factor A, which describes the elastic anisotropy in a cubic structure, is defined as follows:

$$A = 2C_{44}/(C_{11} - C_{12}) \tag{2}$$

For an isotropic material, A = 1 and any deviation from the unity indicates the extent of the elastic anisotropy in a material. For the investigated Na_2Po compound, the calculated value of the anisotropic factor is practically equal to the unity (from Table II), hence, indicating its elastic isotropy characteristics. On the other hand, a simple and practical way to estimate the elastic anisotropy is by utilizing the three-dimensional (3D) closed surface visualization of the elastic moduli corresponding to the material. In the present work, the 3D closed surface of the Young's modulus (corresponding to the Na_2Po compound) is visualized to estimate the elastic anisotropy of the Na_2Po compound. The directional dependence of the Young's modulus in the spherical coordinates for a cubic structure is given by the following equation[44]:

$$1/E = S_{11} - 2(S_{11} - S_{12} - 0.5S_{44})(l_1^2 l_2^2 + l_2^2 l_3^2 + + l_1^2 l_3^2) \tag{3}$$

In this equation, S_{ij} are the elastic compliance constants, and l_1, l_2 and l_3 are the directional cosines with respect to the x, y and z axes, respectively. Equation 3 determines the 3D closed surface and, additionally, the distance from the origin of the system coordinate to this closed surface is equal to the Young's modulus in a given direction. Therefore, in this 3D representation of the Young's modulus, a perfect isotropic system would exhibit a spherical shape and the deviation from a spherical shape indicates the degree of anisotropy in a material. The 3D representation of the Young's modulus of the Na_2Po compound and the cross-section of this closed surface in the xy plane are illustrated in Fig. 2. It is observed that the 3D representation of the Young's modulus corresponding to the Na_2Po compound is spherical, which indicates that the Na_2Po compound displays an isotropic characteristic in the Young's modulus.

Electronic Structure and Density of States (DOS)

The calculated electronic band structure of the sodium polonium Na_2Po compound along high symmetry lines in the first Brillouin zone of the equilibrium crystalline structure is depicted in Fig. 3. It should be noted (to the best of the authors' knowledge) that there are no available experimental or theoretical works in the literature regarding the electronic band structure of the Na_2Po compound that could be compared with the calculated results presented in this article. The overall band profile of the Na_2Po compound is found to have the same characteristic features as observed in the Na_2 (S, Se, Te)[1,2] compounds where analysis of the calculated band structure indicates that the Na_2Po is a direct band gap semiconductor, with the maximum of the valence band and the minimum of the con-

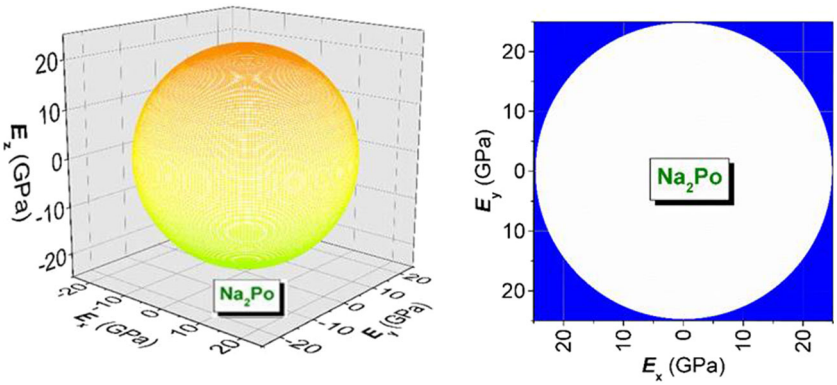

Fig. 2. Calculated 3D stereograms of the Young's modulus and its cross-section in the *xy* plane for the Na_2Po compound.

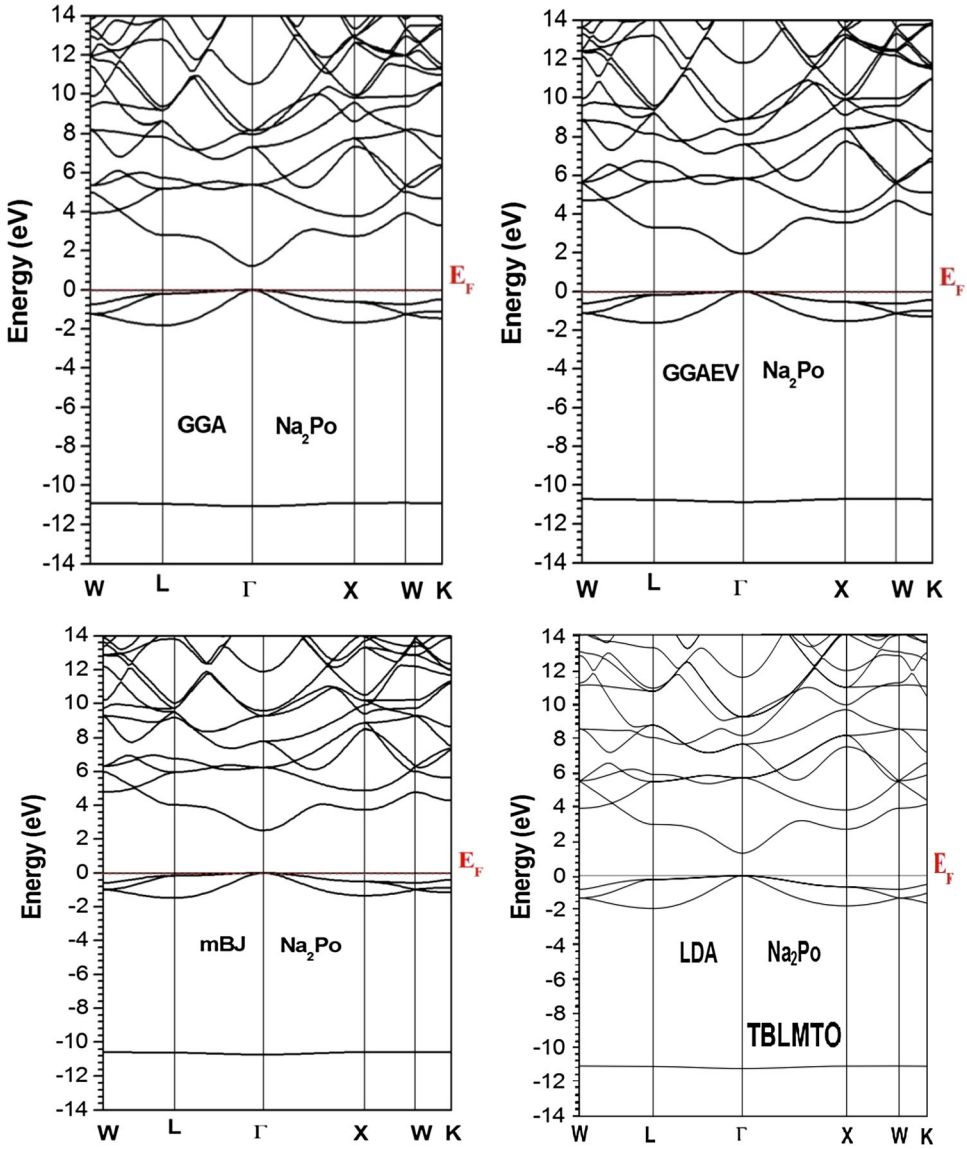

Fig. 3. Electronic energy dispersion curves for Na_2Po along some high symmetry directions in the Brillouin zone within the GGA, GGAEV, mBJ and LDA approximations.

duction band occurring at the Γ symmetry point in the Brillouin zone. The calculated values of the fundamental energy band gap (Γ–Γ) and the indirect energy band gaps (Γ–L) and (Γ–X) of the Na_2Po compound, using four different approximations (LDA, GGA-PBE, GGA-EV and mBJ) for the exchange–correlation potential are given in Table III. It is known that the calculated band gap energies using DFT within the standard LDA and GGA approaches are likely to be approximately 30–50% smaller than the experimental values; therefore, the real band gap energies of the Na_2Po compound is expected to be larger than those values obtained using the common GGA and LDA approaches, as listed in Table III. From Table III, it is observed that the GGA approach underestimates the band gap energy value of the Na_2Po compound by ~51% as compared to the value obtained using the TB-mBJ approach. Hence, the TB-mBJ functional significantly improves the band gap energy value of the Na_2Po compound as compared to the common GGA approach where the calculated band gap energy value is expected to be in agreement with the real value. Additionally, as compared to the other compounds in the series,[2] the Na_2Po compound has the smallest band gap energy.

On the other hand, the calculated electronic bands can be assigned to the different atoms in the compound through the calculation of the total- and atomic-resolved *l*-projected density of states (TDOS and PDOS, respectively) diagrams, as shown in Fig. 4. From Fig. 4, it can be observed that the lowest, deep-lying and very narrow group of valence bands arises from the *s*-like state of the Po atom, and the next-highest occupied valence band arises from the Po *p*-like states. Conversely, the low-lying empty conduction band is an admixture from the Na *s* and Po *sp* states.

Optical Properties

The optical properties of solids can be obtained through the calculation of the complex dielectric function, $\varepsilon(\omega) = \varepsilon_1(\omega) + i\varepsilon_2(\omega)$ and the imaginary part, $\varepsilon_2(\omega)$, of the dielectric function can be computed from knowledge of the electronic band structure of the investigated material. In the limit of linear optics and within the framework of random phase approximation, $\varepsilon_2(\omega)$ can be expressed in the following well-known relation[45]:

$$\varepsilon_2(\omega) = \frac{e^2\hbar}{\pi m^2\omega^2}\sum_{V,C}\int_{BZ}|M_{CV}(k)|^2\delta[\omega_{CV}(k)-\omega]\mathrm{d}^3k \quad (4)$$

where the integral symbol symbolizes integration over the first Brillouin zone, $M_{CV}(k) = \langle u_{Ck}|\mathrm{e}\cdot\nabla|u_{Vk}\rangle$, represents the momentum dipole elements, which represent the matrix elements for the direct transitions between the valence band, $u_{Vk}(r)$, and the conduction band, $u_{Ck}(r)$, states; $\hbar\omega_{CV}(k) = E_{Ck} - E_{Vk}$ provides the corresponding transition energy and e is the potential vector defined by the electric field. Conversely, the real part of the dielectric tensor, $\mathrm{Re}(\varepsilon(\omega)) = \varepsilon_1(\omega)$, can be derived from the imaginary part by employing the Kramers–Kronig relation:

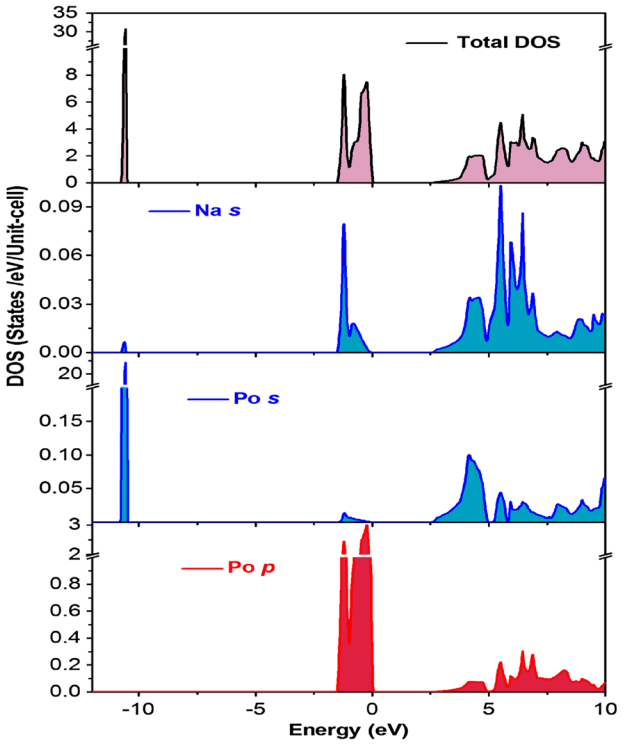

Fig. 4. Calculated total- and atomic-resolved *l*-projected density of states diagrams for the Na_2Po compound.

Table III. Calculated direct (*Γ*–*Γ*) and indirect (*Γ*–L, *Γ*–X) band gaps (in eV) for the Na_2Po compound in an antifluorite-type structure

Used method	E_g (*Γ*–*Γ*)	E_g (*Γ*–L)	E_g (*Γ*–X)
FPLAPW-GGA	1.23	2.81	2.75
FPLAPW-GGAEV	1.94	3.31	3.56
FPLAPW-mBJ	2.52	4.02	3.73
TBLMTO-LDA	1.75	3.33	2.91

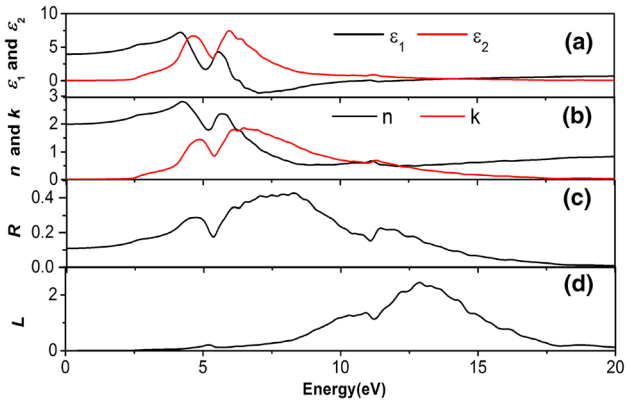

Fig. 5. Calculated real and imaginary parts of the dielectric function ($\varepsilon_1(\omega)$ and $\varepsilon_2(\omega)$; panel a), refractive index and extinction coefficient ($n(\omega)$ and $k(\omega)$; panel b), reflectivity ($R(\omega)$; panel c) energy loss function ($L(\omega)$; panel d) spectrum for Na_2Po.

$$\varepsilon_1(\omega) = 1 + \frac{2}{\pi} P \int_0^{\infty} \frac{\omega' \varepsilon_2(\omega')}{\omega'^2 - \omega^2} \mathrm{d}\omega' \qquad (5)$$

where P indicates the principal value of the integral. Equation 4 yields the unbroadened $\varepsilon_2(\omega)$ spectrum and, consequently, it will have more structures in the spectrum than the experimental ones. In order to compare with the potential experimental findings, the calculated imaginary part of the dielectric function has been broadened with a broadening parameter equal to 0.1.

Figure 5a shows the spectra of the real and imaginary parts of the complex dielectric function versus photon energy up to 20 eV, where the interpretation of the $\varepsilon_2(\omega)$ spectrum in connection with the electronic transitions can be done with the help of the band structure and the DOS, as shown in Figs. 3 and 4, respectively. The imaginary part of the complex dielectric function [$\varepsilon_2(\omega)$] indicates the manner by which the compound absorbs the incident radiation where the lowest energy part of the imaginary spectrum (from 3.0 eV to 7.0 eV) is characterized by two peaks of the highest intensity. These peaks are due to the electronic transitions from the top of the valence band to the isolated, low-energy block in the conduction band. From the generated DOS spectrum in Fig. 4, the first peak located at about 4.7 eV is due to the transitions from the occupied Po-2*p* valence states to the unoccupied Na-*s* conduction states. Furthermore, the second peak centered at about 6.0 eV is dominated by the transitions from the occupied Na-*s* valence states to the unoccupied Po-*s* conduction states as well as from the valence Po-*2p* states to the conduction Na-*s* states.

Knowledge of the imaginary part of the complex dielectric function allows the calculation of its real part (see Fig. 5a) using the Kramers–Kronig relation in Eq. 5, followed by the computation of various optical constants which characterize the propagation of the electromagnetic wave through the material. The static real part of the dielectric function, ε_0, is found to be 3.95 for the Na_2Po compound, which is slightly larger as compared to the Na_2S[2] compound. Furthermore, it can be seen that the main peak in the $\varepsilon_1(\omega)$ spectrum appears at 4.2 eV, followed by a steep decrease and another peak located at 5.7 eV. Following that, the magnitude of the $\varepsilon_1(\omega)$ spectrum becomes negative for the energy range from 6.5 eV to 10 eV, and reaches a minimum value where the $\varepsilon_1(\omega)$ spectrum then subsequently slowly increases in magnitude at high energy.

The refractive index spectrum is related to the linear electro-optical coefficient, which (in turn) determines the photorefractive sensitivity of the crystal, is depicted in Fig. 5b. It is seen that the refractive index increases with photon energy to reach its maximum value at 4.3 in the UV region and the static refractive index, $n(0)$ of the Na_2Po compound is found to be about 2.0.

Figure 5c shows the reflectivity spectrum of the Na_2Po compound, which increases from its static value of about 12% to reach a maximum dynamic reflectivity value of about 43% at the photon energy of about 8.0 eV. This is coincides with the lowest negative value of the $\varepsilon_1(\omega)$ spectrum and, subsequently, the reflectivity magnitude decreases to almost zero for photon energies higher than 18 eV.

The $L(\omega)$ spectrum describes the energy loss of fast electrons passing through a material; hence, the spectrum reflects the features associated with the plasma resonance and the corresponding screened plasma frequency. From Fig. 5d it is observed that the spike in the $L(\omega)$ spectrum for the Na_2Po compound appears at 12.8 eV which corresponds to the abrupt reduction in the reflectance magnitude.

Thermodynamic Properties

From the calculated total energy as a function of the primitive cell volume (*E*–*V*) data by using the FP-LAPW + lo method at zero pressure and temperature, together with the standard thermodynamic relations, some macroscopic physical properties versus pressure and temperature for the Na_2Po compound have been derived.

Temperature effects on the volume (*V*) and bulk modulus (*B*) at some fixed pressures are shown in Fig. 6 where it can be easily observed that at a given pressure, both the volume and bulk modulus parameters are nearly constant for temperature T in the range from 0 K to 50 K. For temperature $T > 50$ K, the volume increases while the bulk modulus decreases with increasing temperature. On the other hand, when the pressure P increases, the volume decreases while the bulk modulus corresponding to the compound increases at a given temperature. Hence, from the above observations in Fig. 6, the compressibility (β) defined as ($\beta = 1/B$) of

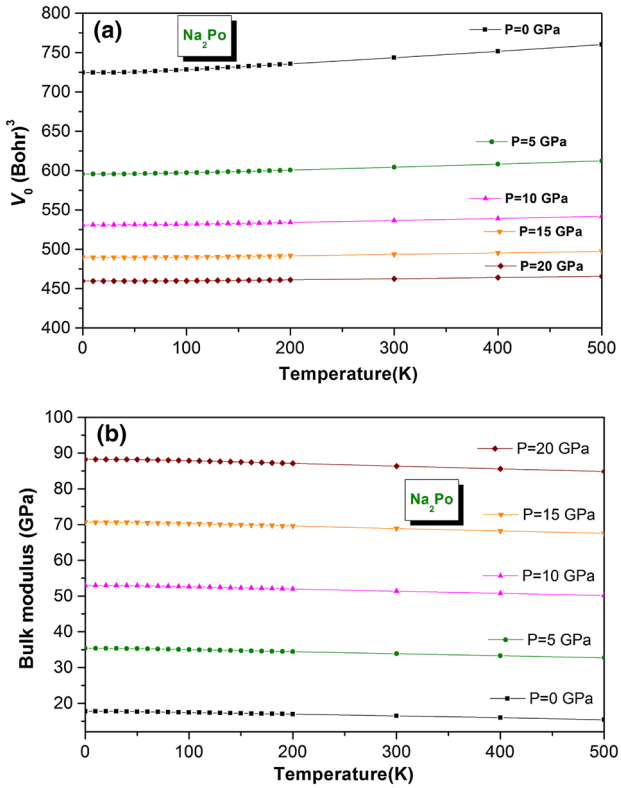

Fig. 6. Variation of the unit cell volume (a) and the bulk modulus (b) versus temperature at some different fixed pressures for Na_2Po.

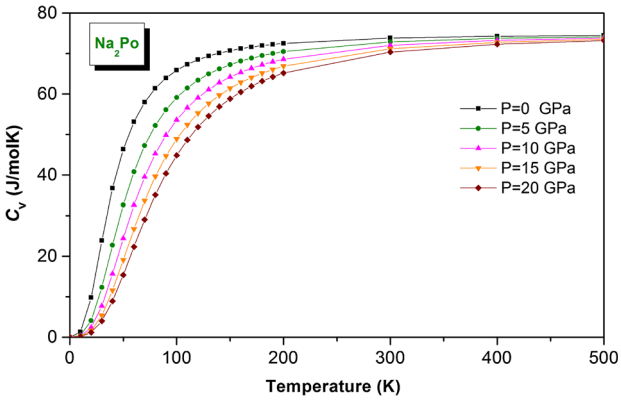

Fig. 7. Variation of the heat capacity C_V versus temperature at some different pressures for Na_2Po.

the Na_2Po compound increases within creasing temperature (above 50 K) at a given pressure and decreases with increasing pressure at a given temperature.

The heat capacity of crystals is an old topic in condensed matter physics which is associated with illustrious names,[46] and the variation of the isochoric heat capacity (C_V) versus temperature at the fixed pressures of 0 GPa, 5 GPa, 10 GPa, 15 GPa and 20 GPa is shown in Fig. 7. It is easily observed that when the temperature increases, the C_V

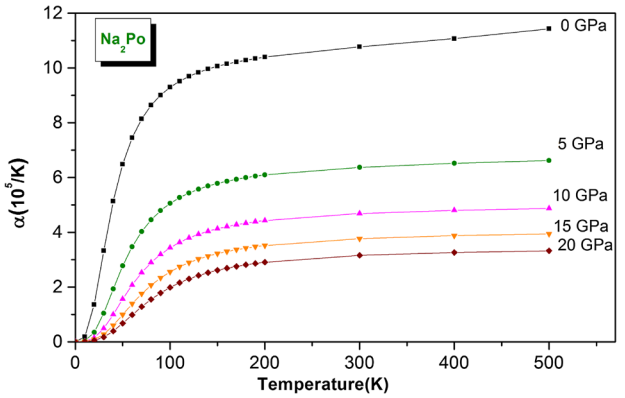

Fig. 8. Variation of the volume expansion coefficient α versus temperature at some different fixed pressures for Na_2Po.

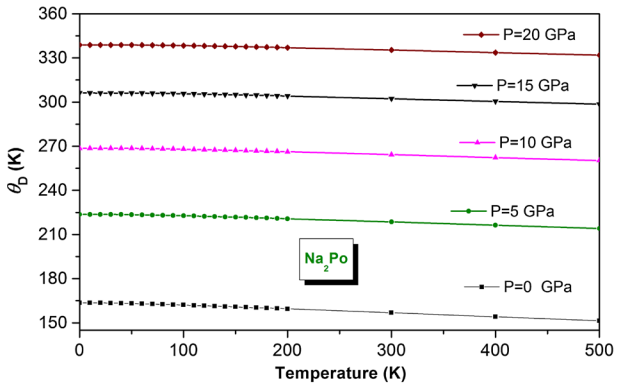

Fig. 9. Variation of Debye temperature versus temperature at some fixed pressures for Na_2Po.

parameter increases rapidly at low temperature, followed by slow increments at the high temperature range and, subsequently, tends to the Petit and Dulong limit,[47] which is a common feature for all solids at high temperature. From Fig. 7 it is clear that when $T < 200$ K, the heat capacity (C_V) depends on both temperature and pressure, whereas at high temperatures, C_V approaches approximately 74.50 J mol^{-1} K^{-1}.

The calculated thermal expansion coefficient (α) at different pressures and temperatures for the Na_2Po compound is shown in Fig. 8. At a given pressure, α increase rapidly with temperature up to 200 K, followed by a slower rate of increase. For $P > 20$ GPa, the value of α at $T = 500$ K is slightly larger as compared to α at 300 K, which indicates that the temperature dependence of α is negligible at higher temperatures and pressures. At ambient conditions, the calculated α of the Na_2Po compound is around 10.77×10^{-5} K^{-1}.

The Debye temperature, being the crucial quantity in the quasi harmonic Debye model, is also associated with many physical properties of solids, such as the heat capacity, elastic constants and melting temperature; the pressure and temperature dependences of

the Debye temperature are shown in Fig. 9. It can be inferred that the calculated value of the Debye temperature at zero pressure and temperature is approximately equal to 163.5 K. Therefore, the Debye temperature decreases almost linearly with increasing temperature at a fixed pressure.

CONCLUSIONS

To summarize, the present work reports a theoretical study of the electronic structure, optical and thermal properties for sodium polonide using both FP-LAPW + lo and TB-LMTO methods within the density functional study. The calculated lattice parameter value is in good agreement with the measured one with a slight overestimation when using FP-LAPW + lo-GGA and slight underestimation using TB-LMTO-LDA. All used approximations for the electronic exchange–correlation potential reveal that sodium polonide is a direct-band gap semiconductor. The single-crystal and polycrystalline elastic constants are numerically estimated. Analysis of the obtained results reveals that Na_2Po is a soft material, being ductile and characterized by isotropic elastic properties. Some macroscopic optical parameters, including dielectric function, refraction index, reflectivity coefficient and energy-loss function, have been predicted. The dependence of the lattice parameter, bulk modulus, heat capacity, volume expansion coefficient and Debye temperature on temperature and pressure have been obtained successfully using the quasi-harmonic Debye model. We hope that the present results would be helpful in analyzing the future experimental measurements of the electronic, optical and thermal properties.

ACKNOWLEDGEMENTS

Authors (R. Khenata, A. Bouhemadou and S. Bin-Omran) acknowledge the financial support by the Deanship of Scientific Research at King Saud University for funding the work through the research group Project No. RPG-VPP-088.

REFERENCES

1. R.D. Eithiraj, G. Jaiganesh, and G. Kalpana, *Int. J. Mod. Phys. B* 23, 5027 (2009).
2. H. Khachai, R. Khenata, A. Bouhemadou, A. Haddou, A.H. Reshak, B. Amrani, D. Rached, and B. Soudini, *J. Phys.* 21, 095404 (2009).
3. E. Zintl, A. Harderand, and B. Dauth, *Z. Elektrochem.* 40, 588 (1934).
4. D. Biseri, A. di Bona, P. Paradisi, and S. Valeri, *J. App. Phys.* 87, 543 (2000).
5. A. Piccioli, R. Pegna, I. Fedorko, M. Giunta, and N. Malakhov, *Nucl. Instrum. Methods Phys. Res. A* 518, 602 (2004).
6. C. Joram, *Nucl. Phys. B* 78, 407 (1999).
7. X. Zhang, C. Ying, H. Ma, G. Shi, and Z. Li, *Phys. Scr.* 88, 035602 (2013).
8. W. Bührer and H. Bill, *Helv. Phys. Acta* 50, 431 (1977).
9. B. Bertheville, H. Bill, and F. Kubel, *J. Phys. Chem. Solids* 58, 1569 (1997).
10. W. Bührer and H. Bill, *J. Phys. C* 13, 5495 (1980).
11. J.C. Schon, Z. Cancarevic, and M. Jansen, *J. Chem. Phys.* 121, 2289 (2004).
12. A. Lichanot, E. Apra, and R. Dovesi, *Phys. Status Solidi (b)* 177, 157 (1993).
13. P. Azavant and A. Lichanot, *Acta Cryst. (A)* 49, 91 (1993).
14. P. Azavant, A. Lichanot, M. Rérat, and C. Pisani, *Acta Cryst. (B)* 50, 279 (1994).
15. H. Khachai, R. Khenata, A. Bouhemadou, A.H. Reshak, A. Haddou, and B. Soudini, *Solid State Commun.* 147, 178 (2008).
16. F. Kalarasse and B. Bennecer, *Comput. Mat. Sci.* 50, 1806 (2011).
17. S.M. Alay-e-Abbasand and A. Shaukat, *J. Mater. Sci.* 46, 10027 (2011).
18. G.K.H. Madsen, P. Blaha, K. Schwarz, E. Sjöstedt, and L. Nordstrom, *Phys. Rev. B* 64, 195134 (2001).
19. K. Schwarz, P. Blaha, and G.K.H. Madsen, *Comput. Phys. Commun.* 147, 71 (2002).
20. P. Hohenberg and W. Kohn, *Phys. Rev. B* 136, 864 (1964).
21. W. Kohn and L.J. Sham, *Phys. Rev.* 140, A113 (1965).
22. P. Blaha, K. Schwarz, G.K.H. Madsen, D. Kvasnicka, and J. Luitz, *WIEN2k, An augmented plane wave plus local orbitals program for calculating crystal properties* (Vienna: Vienna University of Technology, 2001).
23. K.M. Wong, S.M. Alay-e-Abbas, A. Shaukat, Y. Fang, and Y. Lei, *J. Appl. Phys.* 113, 014304 (2013).
24. K.M. Wong, S.M. Alay-e-Abbas, Y. Fang, A. Shaukat, and Y. Lei, *J. Appl. Phys.* 114, 034901 (2013).
25. J.P. Perdew, K. Burke, and M. Ernzerhof, *Phys. Rev. Lett.* 77, 3865 (1996).
26. E. Engel and S.H. Vosko, *Phys. Rev. B* 47, 13164 (1993).
27. F. Tran and P. Blaha, *Phys. Rev. Lett.* 102, 226401 (2009).
28. H.J. Monkhorst and J.D. Pack, *Phys. Rev. B* 13, 5188 (1976).
29. O.K. Andersen, *Phys. Rev. B* 12, 3060 (1975).
30. O.K. Andersen and O. Jepsen, *Phys. Rev. Lett.* 53, 2571 (1984).
31. U. von Barth and L. Hedin, *Phys. C* 5, 1629 (1972).
32. O. Jepsen and O.K. Andersen, *Solid State Commun.* 9, 1763 (1971).
33. M.A. Blanco, E. Francisco, and V. Luaña, *Comput. Phys. Commun.* 158, 57 (2004).
34. M.A. Blanco, A.M. Pendás, E. Francisco, J.M. Recio, and R. Franco, *J. Mol. Struct. Theochem.* 368, 245 (1996).
35. M. Florez, J.M. Recio, E. Francisco, M.A. Blanco, and A.M. Pendás, *Phys. Rev. B* 66, 144112 (2002).
36. H.V. Moyer, *Polonium* (Oak Ridge: United States Atomic Energy Commission, 1956).
37. F. Birch, *J. Geophys. Res.* 83, 1257 (1978).
38. M.J. Mehl, *Phys. Rev. B* 47, 2493 (1993).
39. J. Wang and S. Yip, *Phys. Rev. Lett.* 71, 4182 (1993).
40. J. Haines, J.M. Leger, and G. Bocquillon, *Annu. Rev. Mater. Res.* 31, 1 (2001).
41. S.F. Pugh, *Philos. Mag.* 45, 823 (1954).
42. H. Ledbetter and A. Migliori, *J. Appl. Phys.* 100, 063516 (2006).
43. P. Lloveras, T. Castán, M. Porta, A. Planes, and A. Saxena, *Phys. Rev. Lett.* 100, 165707 (2008).
44. J.F. Nye, *Properties of crystals* (Oxford: Oxford University Press, 1985).
45. C. Ambrosch-Draxl and J.O. Sofo, *Comput. Phys. Commun.* 175, 1 (2006).
46. A. Einstein, *Ann. Phys.* 22, 80 (1907).
47. A.T. Petit and P.L. Dulong, *Ann. Chim. Phys.* 10, 395 (1819).